Received: 18 June 2021 | Revised: 15 December 2021 | Accepted: 17 December 2021

DOI: 10.1002/cne.25293

RESEARCH ARTICLE

JCN RESEARCH IN SYSTEMS NEUROSCIENCE THE JOURNAL OF COMPARATIVE NEUROLOGY WILEY

Differential effects of experimental glaucoma on intrinsically photosensitive retinal ganglion cells in mice

Jingyi Gao[1] | Erin M. Griner[1] | Mingna Liu[1] | Joanna Moy[1] | Ignacio Provencio[1,2,3] | Xiaorong Liu[1,2,3,4]

[1] Department of Biology, University of Virginia, Charlottesville, Virginia, USA

[2] Department of Ophthalmology, University of Virginia, Charlottesville, Virginia, USA

[3] Program in Fundamental Neuroscience, University of Virginia, Charlottesville, Virginia, USA

[4] Department of Psychology, University of Virginia, Charlottesville, Virginia, USA

Correspondence
Ignacio Provencio and Xiaorong Liu, Department of Biology, University of Virginia, Charlottesville, VA 22904, USA.
Email: provencio@virginia.edu and xl8n@virginia.edu

Jingyi Gao, Erin M. Griner, and Mingna Liu contributed equally to this work.

Funding information
NIH, Grant/Award Numbers: R01EY029121, R01EY026286

Abstract

Glaucoma is a group of eye diseases characterized by retinal ganglion cell (RGC) loss and optic nerve damage. Studies, including this study, support that RGCs degenerate and die in a type-specific manner following the disease insult. Here we specifically examined one RGC type, the intrinsically photosensitive retinal ganglion cell (ipRGC), and its associated functional deficits in a mouse model of experimental glaucoma. We induced chronic ocular hypertension (OHT) by laser photocoagulation and then characterized the survival of ipRGC subtypes. We found that ipRGCs suffer significant loss, similar to the general RGC population, but ipRGC subtypes are differentially affected following chronic OHT. M4 ipRGCs, which are involved in pattern vision, are susceptible to chronic OHT. Correspondingly, mice with chronic OHT experience reduced contrast sensitivity and visual acuity. By comparison, M1 ipRGCs, which project to the suprachiasmatic nuclei to regulate circadian rhythmicity, exhibit almost no cell loss following chronic OHT. Accordingly, we observed that circadian re-entrainment and circadian rhythmicity are largely not disrupted in OHT mice. Our study demonstrates the link between subtype-specific ipRGC survival and behavioral deficits in glaucomatous mice. These findings provide insight into glaucoma-induced visual behavioral deficits and their underlying mechanisms.

KEYWORDS
circadian rhythm, glaucoma, intrinsically photosensitive retinal ganglion cells, melanopsin, ocular hypertension, visual acuity

1 | INTRODUCTION

Glaucoma, characterized by retinal ganglion cell (RGC) loss and optic nerve damage, is one of the leading causes of blindness (Tham et al., 2014). RGCs, which exhibit diverse morphologies and functions (Sanes & Masland, 2015), convey photic information from the retina to processing centers in the brain (Quigley, 2016). Studies, including ours, have shown subtype-specific RGC loss in various models of glaucoma and optic nerve injury, yet much remains to be characterized regarding RGC subtype-associated visual deficits and their underlying mechanisms (Cui et al., 2015; Della Santina et al., 2013; Duan et al., 2015; Feng, Zhao et al., 2013, 2017; Chen et al., 2015; Li et al., 2006; Tran et al., 2019).

One type of RGC, the intrinsically photosensitive retinal ganglion cell (ipRGC), plays a role in image-forming and non-image-forming photoreception (Berson et al., 2010; Panda et al., 2002). Although all ipRGCs express the rhabdomeric-like photopigment melanopsin, six distinct subtypes of ipRGCs, M1 through M6, have been described and characterized (Do, 2019; Duda et al., 2020; Tsui et al., 2020). For example, M1 ipRGCs, having dendrites that stratify in the OFF-sublamina of the inner plexiform layer (IPL), express the highest level of melanopsin among the subtypes and exhibit the most robust intrinsic

light response (Emanuel et al., 2017). M1 cells project primarily to the hypothalamic suprachiasmatic nuclei (SCN) (Berson et al., 2010), mediating the effects of light on circadian regulation of physiology and behavior (Baver et al., 2008; Berson et al., 2002; Chen et al., 2011). By contrast, the M4 ipRGCs, also known as the sustained large ON-alpha RGCs, are weakly melanopsin positive and project to the ventromedial sector of the dorsolateral geniculate nucleus (dLGN), a site responsible for some aspects of pattern vision such as contrast sensitivity (Ecker et al., 2010; Estevez et al., 2012; Schmidt et al., 2014).

How ipRGCs are affected by glaucomatous insult remains an area of great interest. Subtype-dependent ipRGC survival has been studied in various animal models, although the results among different studies have been equivocal. For example, in a rat ocular hypertension (OHT) model, few if any melanopsin-positive ipRGCs degenerated (Li et al., 2006). However, in mice following optic nerve crush injury, most M2 ipRGCs died, but more than 70% of M1 ipRGCs survived (Duan et al., 2015). Furthermore, physiological deficits associated with ipRGC loss have been examined in glaucoma patients and animal models. Glaucoma patients often suffer a higher prevalence of sleep disorders, which may be due to the general loss of ipRGCs (Ciulla et al., 2020; Gracitelli et al., 2015). The pupillary light reflex, regulated by ipRGCs, was reduced in humans with glaucoma (Gracitelli et al., 2015). In a rat model of experimental glaucoma, animals can synchronize their locomotor activities to the light: dark (LD) cycle, but they require more days to entrain to a shifted LD cycle in comparison to control rats (Drouyer et al., 2008). Yet much remains to be characterized regarding the functional changes resulting from the subtype-specific loss of ipRGCs during glaucoma development and progression.

In this study, the subtype-specific ipRGC loss and the attendant functional deficits in a mouse model of experimental glaucoma were examined. Long-term OHT was induced by laser photocoagulation, and the survival of ipRGC subtypes was characterized. Furthermore, the functional consequences on circadian rhythmicity, visual acuity, and contrast sensitivity were analyzed.

2 | MATERIALS AND METHODS

2.1 | Laser-photocoagulation to induce chronic OHT in mice

Adult (3–14 months) male and female wild-type (WT) C57BL/6 mice were used in this study. OHT was generated by laser photocoagulation of the trabecular meshwork of the eyes in 2–3 months old mice as described previously (Feng, Chen, et al., 2013; Feng et al., 2016; Chen et al., 2015). In brief, mice were anesthetized by intraperitoneal injection of 80 mg/kg ketamine (Kataset, Zoetis; NADA #043-304) and 4 mg/kg xylazine (AnaSed, Akorn; NADA#139-236). Eyes were dilated with topical application of 2.5% phenylephrine hydrochloride ophthalmic solution (Akorn, NDC #17478-201-15) and 1% tropicamide ophthalmic solution (Akron, NDC # 17478-102-12), and the aqueous humor was aspirated from the anterior eye by a glass micropipette (World Precision Instruments Inc., Sarasota, FL, USA). Laser illumination was delivered unilaterally or bilaterally (Figure 1) by the PASCAL Synthesis 532 system (Topcon, Oakland, NJ, USA). Six groups of five 200 μm (diameter) laser spots with zero spacing were applied perpendicular to the corneal limbus to circumscribe the trabecular meshwork at a laser power of 120 mW and exposure time of 20 ms. This procedure took 10–15 min for each eye. A drop of VIGAMOX (moxifloxacine hydrochloride ophthalmic solution 0.5%) was applied to prevent infection, and lubricants were applied (Puralube Vet ointment, NDC # 17033-211-38) to prevent drying and formation of a cataract. The animals then were kept on a heating pad until fully responsive.

2.2 | Intraocular pressure measurement and the optomotor test

Intraocular pressure (IOP) was measured in awake mice using a Tonolab rebound tonometer (iCare, Raleigh, NC, USA) as previously described (Feng, Chen, et al., 2013; Thomson et al., 2020). In brief, each mouse was placed into a soft plastic cone holder and restrained on a platform. Averages from three sets of measurements per eye were recorded. All IOP measurements were obtained under ambient lighting between 10:00 a.m. and 1:30 p.m.

Both visual acuity and contrast sensitivity were assessed by the optomotor test (Rangarajan et al., 2011; Thomson et al., 2020) (PhenoSysqOMR, PhenoSys GmbH, Berlin, Germany). In the optomotor test, the freely moving animal was placed on a stationary round platform in the middle of four LCD monitors (Thomson et al., 2020). After 1–3 min of adaptation with a gray screen, a sine wave grating was made to move across all four monitors. The animal was presented with moving gratings, which alternated clockwise and counterclockwise for 10 s in each direction with varied spatial frequencies from 0.05 to 0.50 cycles/degree (c/d). The movement of the animal's head in concert with the drifting grating was scored as "seen"; the highest spatial frequency "seen" was defined as the animal's visual acuity. The two eyes of individual mice were examined separately by reversing the drifting grating direction (i.e., a clockwise drifting grating was used to identify the visual function of the left eye, and a counterclockwise drifting grating for the right eye) (Douglas et al., 2005; Feng, Chen, et al., 2013; Feng et al., 2016; Chen et al., 2015). Contrast sensitivity was measured at two preselected frequencies: 0.103 and 0.192 c/d, each with contrasts from 1 to 0.1, defined as the Michelson contrast from the screen's luminance (maximum – minimum)/(maximum + minimum). The contrast threshold for each eye is defined as the lowest contrast that elicits responses at the prefixed frequency, and contrast sensitivity is the reciprocal of the threshold (Prusky et al., 2004).

2.3 | Immunohistochemistry and confocal imaging

Mice were euthanized with 600 mg/kg euthasol (Euthasol, Virbac ANADA, # 200-071) and perfused with 4% paraformaldehyde (PFA) (ChemCruz, sc-281692). Eye cups were dissected, postfixed in PFA for 30 min, washed with phosphate-buffered saline containing Triton-X

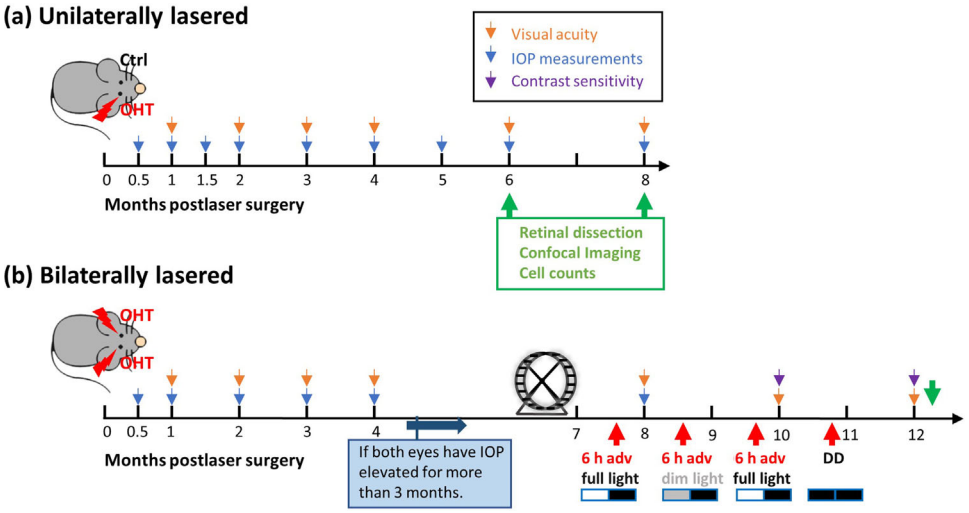

FIGURE 1 Experimental design to investigate ipRGC survival and its functional consequences in laser-induced ocular hypertensive (OHT) mice. (a) Unilaterally lasered mice were generated for cell quantification. OHT was induced in one eye while the other eye of the mouse was used as a control. (b) Bilateral OHT was induced in both eyes of a mouse for circadian behavioral tests. Mice that had IOP consistently elevated for more than 3 months were subjected to three rounds of phase advances (red arrows) in the light period of LD cycle. Free runs under constant darkness (DD) were performed to assess circadian periods at the end. IOP (blue arrows), visual acuity (orange arrows), and contrast sensitivity (purple arrows) were assessed regularly. Adv: advance

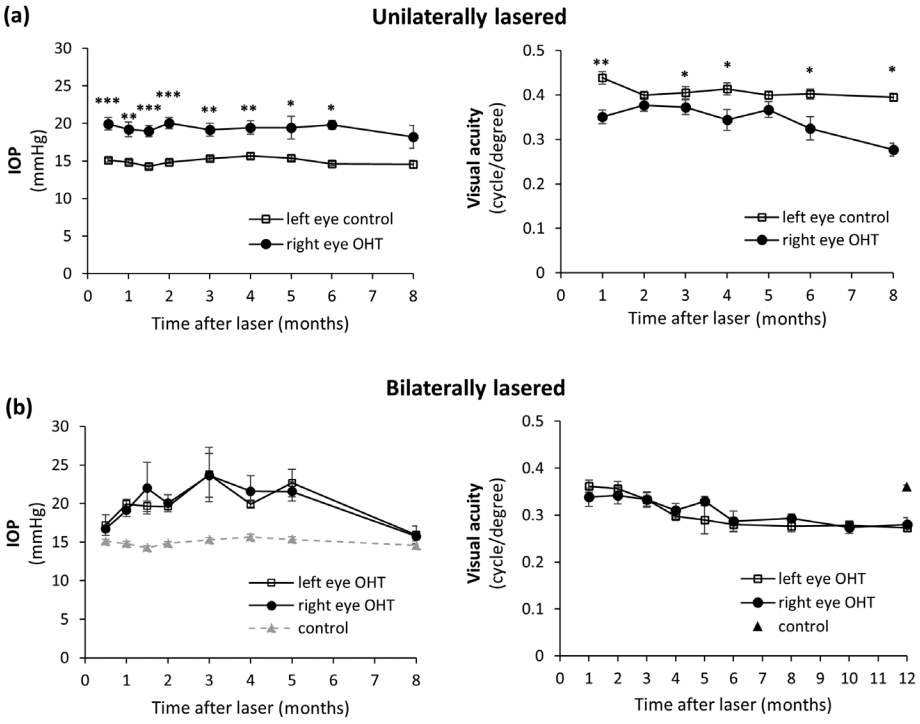

FIGURE 2 Chronic IOP elevation led to decreased visual acuity. (a) For unilaterally lasered mice, the IOP of the OHT eye was elevated for more than 3 months while that of the control eye remained constant (left). With chronic IOP elevation, the visual acuity of the OHT eye continued to decrease while that of the control eye remained relatively stable (right). $n = 4–13$ in each group. (b) For bilaterally lasered mice, the IOP of both OHT eyes (left) remained elevated for more than 3 months. The IOP of control eye from unilaterally lasered mice was shown in gray (dashed line) for purpose of comparison. With chronic IOP elevation, the visual acuity (right) of both eyes continued to decrease. The visual acuity of age matched untreated control mice was shown (black triangle). $n = 4–11$ in each group. $^{*}p < .05$; $^{**}p < .01$; $^{***}p < .001$. in the Mann–Whitney test. Data presented as mean ± *SEM*. If no asterisk, not significant

detergent (PBST, 0.5% Triton X-100), and then blocked for 1 h in blocking buffer (1% BSA and 10% normal donkey serum, 0.5% Triton X-100 (Sigma-Aldrich, St. Louis, MO, USA)). Primary antibodies, diluted using blocking buffer, included a rabbit polyclonal anti-melanopsin (1:2000) (Panda et al., 2002), mouse anti-SMI-32 (Biolegend, 801702/01, 1:250, RRID: AB_2715852), mouse anti-Brn3a (Millipore, MAB1585, 1:125, RRID: AB_94166), and rabbit anti-rbpms (Abcam, ab194213, 1:500). Secondary antibodies, including donkey anti-mouse immunoglobulin G conjugated to Alexa Fluor 594 dye (Invitrogen A-21203, RRID: AB_141633), donkey anti-mouse immunoglobulin G conjugated to Alexa Fluor 647 dye (Invitrogen A-31571, RRID: AB_162542), and donkey anti-rabbit immunoglobulin G conjugated to Alexa Fluor 488 dye (Invitrogen A-21206, RRID: AB_2535792), were also diluted at 1:1000 in blocking buffer and incubated overnight at 4°C. After immunostaining, retinas were flat mounted and cut into four quadrants: temporal, nasal, inferior, and superior. For cryosection, fixed eye cups were cryoprotected overnight in 30% sucrose solution and embedded in optimal cutting temperature compound (OCT) medium (Sakura Finetek, Torrance, CA, USA). Blocks were sectioned by cryostat at 15–20 μm and counterstained with DAPI (Vectashield H-1200, Vector Laboratories, Inc. Burlingame, CA, USA).

Confocal images were taken using a Zeiss LSM800 confocal microscope (Zeiss, Thornwood, NY, USA). For flat-mounted retinas, Z-stack images covering the depth of the retina from the inner nuclear layer (INL) to the ganglion cell layer (GCL; approximately 50–80 μm) were acquired. Lower magnification (5×) images were captured for each leaflet of the retina using the tiling/stitch function in Zen (Zen 3.2; Oberkochen, Germany; http://www.zeiss.com/microscopy/en_us/products/microscope-software/zen.html#introduction; RRID: SCR_013672). For cell counting, individual images were captured at 20×, covering an area of 0.102 mm^2. To distinguish the M1 cells in the GCL from the displaced M1s in the INL, individual z-stack images covering an area of 0.0255 mm^2 were taken using a 40× water immersion objective. Three-dimensional (3D) reconstruction and vertical view images were done and acquired by Imaris (Imaris 9.6, Bitplane Inc. Concord, MA, USA; http://www.bitplane.com/imaris/imaris; RRID: SCR_007370).

2.4 | Antibody characterization

Primary antibodies are listed in Table 1. The primary polyclonal antiserum (UF006) to melanopsin was raised in rabbit against a synthetic peptide consisting of the 15 N-terminal amino acids of mouse melanopsin (Genbank accession NP_038915) conjugated to keyhole limpet hemocyanin (KLH). Specificity of this antiserum has been confirmed in control studies showing a dose-dependent loss of immunoreactivity by preabsorption with the immunogen and by the lack of immunoreactivity in the retinas of melanopsin-null mice (Panda et al., 2002). The lack of immunoreactivity in melanopsin knockout mice was confirmed using the immunoperoxidase method (Panda et al., 2002). We also validated the antibody using the *Opn4*$^{cre/cre}$ *mice* (Ecker et al., 2010) crossed with a Synaptophysin-tdTomato cre reporter line, Ai34(RCL-Syp/tdT)-D (PubMed ID: J:170755). We found some of tdTomato+ cells are strongly SMI-32 positive and weakly melanopsin positive (data not shown), confirming their identity as M4 cells.

The mouse anti-Brn3a antibody (Millipore, #MAB1585, RRID: AB_94166) was generated against amino acids 186–224 of Brn3a fused to the T7 gene 10 protein. According to the manufacturer, it does not recognize either Brn3b or Brn3c, nor stains tissues of Brn-3a knockout mice. This antibody labels RGCs in mouse retina (Voinescu et al., 2009), as seen in this study. We also colabeled Brn3a with rbpms, another general RGC marker, and found that all Brn3a-positive cells were rbpms-positive (Figure 3a).

The mouse anti-SMI-32 antibody (Biolegend, #801702, RRID: AB_2715852) specifically recognizes a 200-kD nonphosphorylated epitope in neurofilament H, tested in various mammalian species. Specifically, in retina it labels some RGC bodies, dendrites, and axons (Feng, Zhao, et al., 2013).

The rabbit anti-rbpms antibody (Abcam, ab194213) was generated against a synthetic peptide within rat rbpms (N-terminal) conjugated to KLH. In western blots, the rbpms antibody detects the expected 22 kDa band from rat heart lysate (manufacturer's specification). In mouse retina, it specifically labels RGCs (Thomson et al., 2020).

2.5 | Cell quantification

For general RGC and ipRGC cell counting, mouse retinas were immunostained with anti-rbpms, anti-Brn3a, or anti-melanopsin antibodies. For each retina, at least 24 *en face* z-stack images covering the depth from the GCL to the INL were captured (roughly 50–80 μm of total depth). Six images were acquired for each quadrant to ensure broad coverage of the entire retina (Figure 1a). A rectangle covering no less than 0.025 mm^2 area was randomly drawn on the images and Brn3a-, rbpms-, or melanopsin-positive cells within the rectangle were manually counted in Zen (Zen 3.2; Oberkochen, Germany).

To quantify M4 cells, mouse retinas were double immunostained with anti-SMI-32 and antimelanopsin antibodies. Images were acquired as described above, and cells were classified as M4 when they met the following three criteria: (1) a cell soma size larger than 200 μm^2, (2) faintly positive label for melanopsin, and (3) strongly positive label for SMI-32.

M1 in the GCL and displaced M1 cells in the INL were counted by taking images at the focal plane of the GCL and INL, respectively. For each retina, a total of 36 *en face* z-stack images were taken with six images for each quadrant. 3D reconstruction was done using Imaris software (Imaris 9.6, Bitplane Inc. Concord, MA,USA) and melanopsin-positive cells with dendrites reaching only the OFF sublamina of the IPL were counted as M1 cells. Although M6 ipRGCS also have dendrites reaching the OFF sublamina of the IPL, they are rarely labeled by immunofluorescence, even with amplification, and therefore are unlikely be misidentified as M1 (Quattrochi et al., 2019). Similarly, cells with at least one dendrite terminating in the ON sublamina of IPL, potentially M3 cells, were not included. Cell density for each retina was calculated using the total number of cells counted divided by the total area.

TABLE 1 Primary antibodies used in this study

Antibody	Immunogen	Source (RRID number)	Dilution factor
Melanopsin	15 N-terminal amino acids of mouse melanopsin	Ignacio Provencio (Panda et al., 2002), rabbit monoclonal	1:2000
Brn3a	Amino acids 186–224 of Brn-3a fused to the T7 gene 10 protein	Millipore, MAB1585, (RRID: AB_94166), mouse monoclonal	1:125
SMI-32	Neurofilament H	Biolegend, 801702, (RRID: AB_2715852), mouse monoclonal	1:250
Rbpms	Synthetic peptide within rat RBPMS (N terminal) conjugated to keyhole limpet hemocyanin	Abcam, ab194213, rabbit polyclonal	1:500

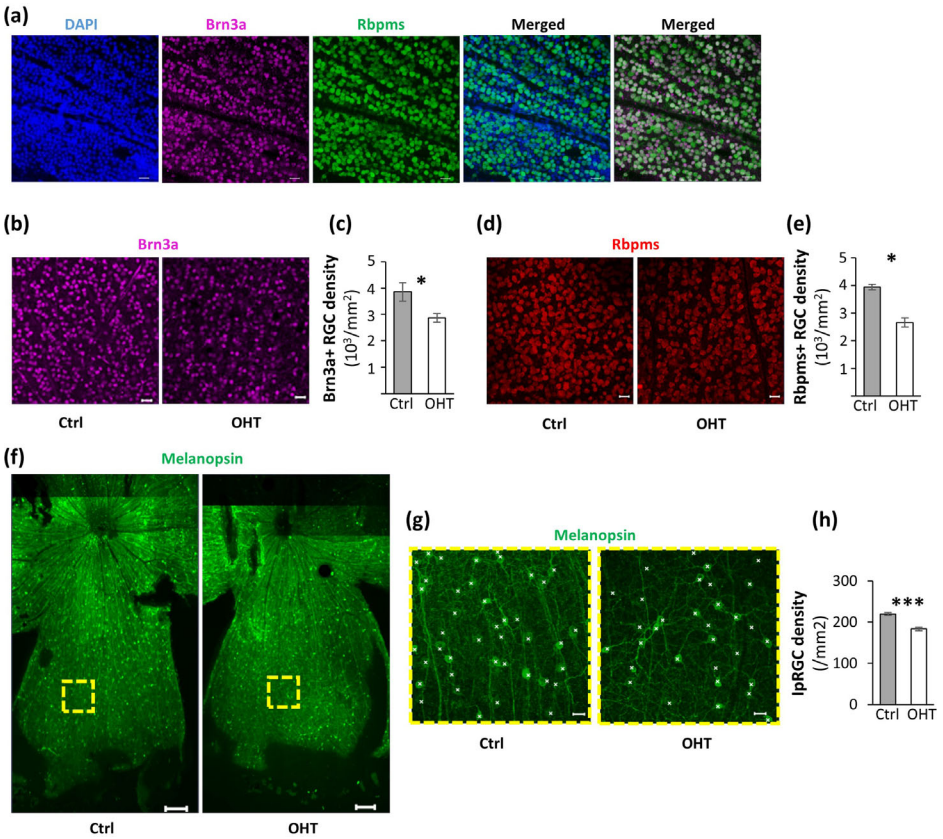

FIGURE 3 General RGC population and ipRGCs suffered significant loss in OHT mice. (a) Flat-mounted retinas of 8-month-old WT mice stained with DAPI (blue), Brn3a (purple), and rbpms (green). Almost all Brn3a-positive cells were rbpms positive and roughly 90% of rbpms-positive cell were Brn3a-positive. (b) Flat-mounted retinas of a control and an OHT eye 6–8-months post laser surgery were immunostained with Brn3a (b) or rbpms (d) antibodies for the general population of RGCs. Quantification of Brn3a-positive cells (c) and rbpms-positive cells (e) were shown between control and OHT retinas. (f) Flat-mounted images of the temporal leaflet of a control (left) and an OHT (right) retina stained with antimelanopsin antibody. (g) The high-magnification images of ipRGCs in the GCL (yellow rectangles in f) were used for cell counting. White crosses denote ipRGC somas. (h) Quantification of melanopsin-positive ipRGCs. *$p < .05$; ***$p < .001$ in the Mann–Whitney test. Scale bar for (a), (b), (d), and (g) is 20 μm and for (f) is 200 μm

2.6 | Circadian behavioral analysis

Animals were housed in individual cages with running wheels in light tight boxes under a 12h:12h L:D schedule. Fluorescent lights (100 μW/cm^2) were used for illumination and food and water were provided ad libitum. Wheel running was monitored and analyzed with the ClockLab collection and analysis software suite (Actimetrics, Wilmette, IL, USA). After at least 14 days of entrainment to the LD cycle, the dark

period was advanced by 6 h and wheel running was monitored for the following 15 days. The duration of re-entrainment was defined as the number of days required to shift activity onset by 6 h followed by two consecutive days of activity onset or offset within this range. Activity onset was determined by the ClockLab software and adjusted manually to avoid masking effects. Entrainment was scored manually by a blind observer.

Circadian phase shifting using low intensity light was performed in a similar manner, except during the 12-h light period, the intensity of the fluorescent source was adjusted to 1.5 $\mu W/cm^2$ by wrapping the fluorescent light bulbs with layers of pliable, semitranslucent neutral density filters.

Animals were also exposed to constant darkness (DD), and the free-running period was calculated according to the onset of activity across at least 10 days in constant darkness. The circadian period was calculated by 24 h minus the slope of the least square fitted line of the onsets.

All results were expressed as the mean±SEM. Nonparametric Mann–Whitney tests were performed to compare two groups of samples. All animal procedures were approved by the Institutional Animal Care and Use Committee at University of Virginia and conformed to the guidelines on Use of Animals from the National Institute of Health (NIH).

3 | RESULTS

3.1 | The general RGC population suffers a significant loss following chronic OHT

We performed laser photocoagulation in adult C57BL/6 mice to induce OHT as described previously (Feng, Chen, et al., 2013; Feng et al., 2016; Chen et al., 2015) (Figure 1). For unilaterally lasered mice, the right eye was lasered and the left untreated eye of the same mouse was used as a control (Figure 1a). We also generated bilaterally lasered mice in order to induce chronic OHT in both eyes for circadian behavioral tests (Figure 1b). We tracked the IOP every 2 weeks for the first 2 months and then every month up to 1 year, and simultaneously tracked visual acuity of each eye. The unilaterally lasered mice with treated eyes that exhibited consistently elevated IOP for more than 3 months and showed declining visual acuity were used for cell quantification (Figure 1a), while bilaterally lasered mice were used for circadian behavioral tests (Figure 1b).

The changes in IOP and visual acuity were tracked over time (Figure 2). For the first 3 months post laser photocoagulation, the IOP of the lasered eye was elevated more than 25% than that of the control eye (Figure 2a). Three months post laser photocoagulation, the IOP of the lasered eye of the unilaterally lasered mice was elevated to 19.15 ± 0.84 mmHg ($n = 7$), significantly higher than that of the nonlasered control eyes (15.31 ± 0.29 mmHg, $n = 7$, $p < 0.01$, Mann–Whitney test; Figure 2a). The IOP of the lasered eye gradually dropped and was not significantly different from the control eyes by 8 months post laser surgery (controls: 14.6 ± 0.5 mmHg, $n = 4$; OHT: 18.2 ± 3.7 mmHg, $n = 6$, $p = .2$, Mann–Whitney test). The IOP was also elevated in each eye of the bilaterally lasered mice for more than 3 months (left panel, Figure 2b) and eventually dropped at 8 months post laser photocoagulation (left eye OHT: 15.94 ± 1.18 mmHg, right eye OHT: 15.77 ± 1.54 mmHg, $p = .87$, Mann–Whitney test; Figure 2b).

Chronic IOP elevation induced a continuous decrease in visual acuity (Figure 2a). The acuity of the OHT eyes dropped from 0.35 ± 0.02 c/d ($n = 11$) to 0.28 ± 0.02 c/d ($n = 6$) at 8 months post laser photocoagulation. At the same time, the control eyes' acuity remained within normal range at 0.39 ± 0.01 c/d ($n = 4$) 8 months post laser surgery, significantly higher than the OHT eyes' ($p = .01$, Mann–Whitney test) (Douglas et al., 2005; Feng, Chen, et al., 2013; Feng et al., 2016; Chen et al., 2015; Prusky et al., 2004).

Next, RGC loss following chronic IOP elevation was quantified. The general RGC population was immunolabeled using antibodies to Brn3a (Xiang et al., 1995) and rbpms (Rodriguez et al., 2014). Previous studies suggested that rbpms is expressed exclusively in most if not all RGCs, while Brn3a is expressed in some RGCs (Feng, Zhao, et al., 2013; Pan et al., 2005; Rodriguez et al., 2014). We confirmed the labeling pattern in WT mice (Figure 3a). It was estimated that about 59% of the cells in the GCL are displaced amacrines and 41% are RGCs (Jeon et al., 1998). Indeed, we found that about 48.2% of all cells in the GCL were rbpms-positive RGCs; in addition, all Brn3a-positive cells were rbpms-positive, while about 87% of rbpms-positive cells were Brn3a-positive (Figrue 3a). At 6 months post laser photocoagulation, the densities of Brn3a-positive cells were quantified and compared between OHT and control eyes (Figure 3b,c). We found that Brn3a-positive RGC density (see Table 2) was significantly reduced by 25.6% in OHT eyes compared to controls (controls: 3859.7 ± 156.8 /mm^2, $n = 5$; OHT: 2871.7 ± 94.4 /mm^2, $n = 3$, $p = .04$, Mann–Whitney test). At 8-months post laser photocoagulation, rbpms-positive RGC density was also significantly reduced by 32.6% in OHT eyes compared to the controls (controls: 3942.5 ± 100.4 /mm^2, $n = 3$; OHT: 2658.1 ± 216.0 /mm^2, $n = 4$, $p = .03$, Mann–Whitney test) (Figure 3d,e). Together our results showed that 6–8 months of chronic IOP elevation induced approximately 25–33% RGC loss, consistent with our previous findings (Feng, Zhao, et al., 2013; Chen et al., 2015).

3.2 | Significant loss of ipRGCs occurs following chronic OHT

Previously studies, including ours, showed that the RGC degeneration is cell type-specific (Duan et al., 2015; Feng, Zhao, et al., 2013). For instance, ipRGCs have been shown to be relatively resistant to chronic OHT or acute optic nerve damage (Duan et al., 2015; Li et al., 2006). Therefore, we next examined whether ipRGC survival differs from survival of the general RGC population in our chronic model of OHT. Melanopsin antisera was used to label the majority of ipRGCs, M1 through M4, and possibly some weakly melanopsin-positive M5 and M6 (Figure 3f,g) (Quattrochi et al., 2019; Stabio et al., 2018). We have included all cells immunolabeled with the anti-melanopsin antisera in the GCL and the INL for general ipRGC quantification. Surprisingly,

TABLE 2 Summary of RGC density in OHT and control mice

RGC type	Cell density (/mm^2) mean ± *SEM* (*n*)		
	Control	OHT (6–9 m post laser photocoagulation)	Percentage change
Rbpms	3942.5 ± 100.4 (3)	2658.1 ± 216.0 (4)	−32.6
Brn3a	3859.7 ± 156.8 (5)	2871.7 ± 94.4 (3)	−25.6
Melanopsin	219.6 ± 3.0 (16)	183.4 ± 4.5 (11)	−16.5
M1	54.4 ± 3.1 (3)	56.4 ± 1.1 (4)	3.4
Displaced M1	7.0 ± 0.7 (16)	6.7 ± 1.0 (12)	−4.2
M4 (SMI-32 + melanopsin)	52.2 ± 2.0 (10)	38.8 ± 2.7 (10)	−25.7
M2, M3, and some M5, M6	106.0[†]	81.5[a]	-23.1

[a]Numbers are based on calculations, not direct cell counts.

at 8–9 months post laser surgery, we observed a 16.5% reduction (Table 2) in the total ipRGC population in the OHT eyes compared to the control eyes (controls: 219.6 ± 3.0 /mm^2, $n = 16$; OHT: 183.4 ± 4.5 /mm^2, $n = 11$, $p < .001$, Mann–Whitney test) (Figure 3f,h). We conclude that, like the general RGC population, the ipRGC population also suffers significant degeneration following the chronic hypertension insult, albeit to a lesser extent. Because the ipRGCs are not a homogeneous group and can be further classified into several subtypes, from M1 to M6, each with distinct morphology and function (Do, 2019), we next examined how different ipRGC subtypes survive in the context of chronic OHT.

3.3 | M4 ipRGCs are susceptible to chronic IOP elevation

Combining immunohistochemistry and 3D reconstruction of ipRGC morphology, we characterized and quantified several ipRGC subtypes. To identify the M4 ipRGCs, we double-stained retinas with antibodies against melanopsin and the SMI-32 neurofilament epitope (Figure 4a). We compared the survival rate of M4 ipRGCs at 8–9 months post laser photocoagulation. We found that M4 ipRGCs were significantly reduced by 25.7% (controls: 52.2 ± 2.0 /mm^2, $n = 10$; OHT: 38.8 ± 2.7 /mm^2, $n = 10$, $p < .01$, Mann–Whitney test) (Figure 4b, Table 2),

Because M4 ipRGCs are thought to be involved in image-forming vision, especially in contrast sensitivity (Schmidt et al., 2014), we tested the contrast sensitivity of the OHT eyes at the spatial frequencies of 0.103 and 0.192 c/d. We found that the contrast sensitivities were significantly reduced (0.192: $p < .01$, and 0.103: $p < .001$ in the Mann–Whitney test) in OHT eyes compared to control eyes (Figure 4c). At 0.103 c/d, the average contrast sensitivity for control eyes was 6.09 ± 0.56, while for the OHT eyes it was 3.15 ± 0.20 ($n = 12$ in each group). At 0.192 c/d, the average contrast sensitivity for the control eyes was 5.50 ± 0.35, while in the OHT eyes it was only 3.63 ± 0.31. This reduction in contrast sensitivity is consistent with the significant loss of general RGCs and M4 ipRGCs.

3.4 | M1 ipRGCs are resistant to chronic IOP elevation

Based on the 3D reconstruction of confocal z-stack images of ipRGCs, we identified common M1 ipRGCs with dendrites reaching the OFF sublamina of the IPL (Figure 5a). A small group of M1 cells also have perikarya located in the INL and thus are called displaced M1 ipRGCs (Figure 5b) (Berson et al., 2010; Duda et al., 2020; Ecker et al., 2010). We quantified the common M1 ipRGCs with cell bodies in the GCL and the displaced ipRGCs separately. Interestingly, we found that the density of M1 ipRGCs in the GCL did not change significantly at 8 months post-IOP elevation compared to controls (controls: 54.4 ± 3.1 /mm^2, $n = 3$; OHT: 56.4 ± 1.1 /mm^2, $n = 4$ $p = .86$, Mann–Whitney test) (Figure 5c). Similarly, we found no significant change in the density of displaced M1 ipRGCs (OHT: 6.7 ± 1 /mm^2, $n = 12$; controls: 7.0 ± 0.7 /mm^2, $n = 16$, $p = .66$, Mann–Whitney test) (Figure 5d). Taken together, the M1 ipRGC population suffered little, if any, cell loss following chronic OHT.

3.5 | Circadian re-entrainment and circadian rhythmicity remain largely intact in OHT mice

Given that M1 ipRGCs are known to innervate the master circadian clock in the hypothalamic SCN (Baver et al., 2008; Hattar et al., 2002; Jain et al., 2012; Chen et al., 2011), and M1 ipRGCs are preferentially spared from damage in OHT mice, we tested the hypothesis that the circadian behaviors may remain largely unaffected in glaucomatous mice. We performed bilateral laser photocoagulation on both eyes of C57BL/6 mice, and then tracked the IOP, visual acuity, and contrast sensitivity for up to 1 year. Mice that showed sustained IOP elevation for more than 3 months for both eyes (Figure 2b) were used for circadian studies. Out of more than 40 mice upon which we performed bilateral laser surgeries, six met this criterion for circadian testing (Figure 1b).

At 7 months post laser photocoagulation, six bilaterally lasered mice and six age-matched control mice were transferred to individual cages

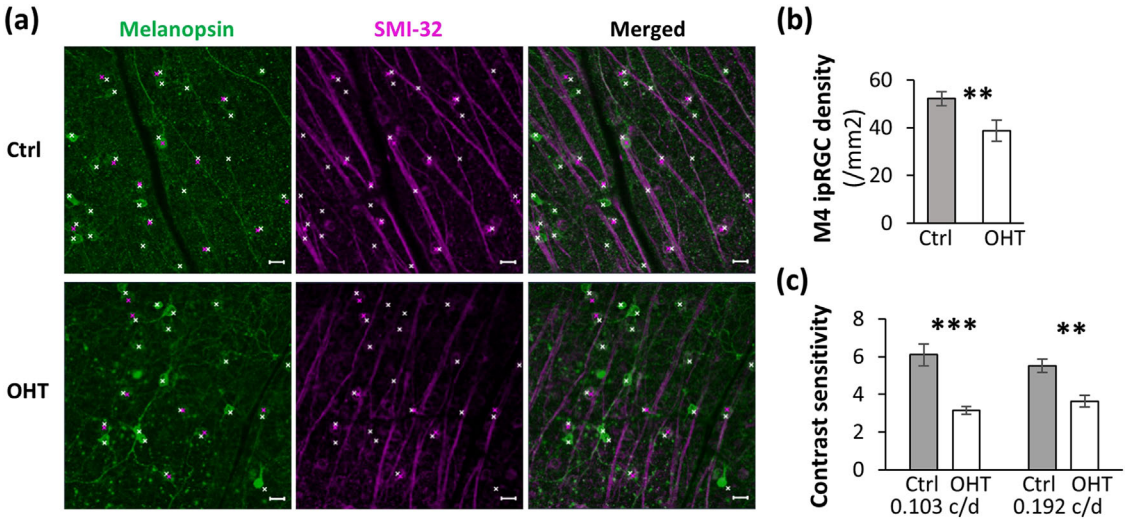

FIGURE 4 M4 ipRGC suffered significant loss following chronic IOP elevation. (a) Confocal images of flat-mounted retinas from a control eye and an OHT eye 8-months postsurgery immunostained with melanopsin and SMI-32 antibodies. White crosses denote melanopsin-positive cells and violet crosses denote large cells positive for both melanopsin and SMI-32. Scale bar is 20 μm. (b) Quantification of M4 cell density in control and OHT retinas. (c) Contrast sensitivity measured at 0.103 and 0.192 cycle per degree (c/d) of control and OHT group 8-months post laser surgery. $^{**}p < .01$; $^{***}p < .001$ in the Mann–Whitney test. Data presented as mean ± *SEM*.

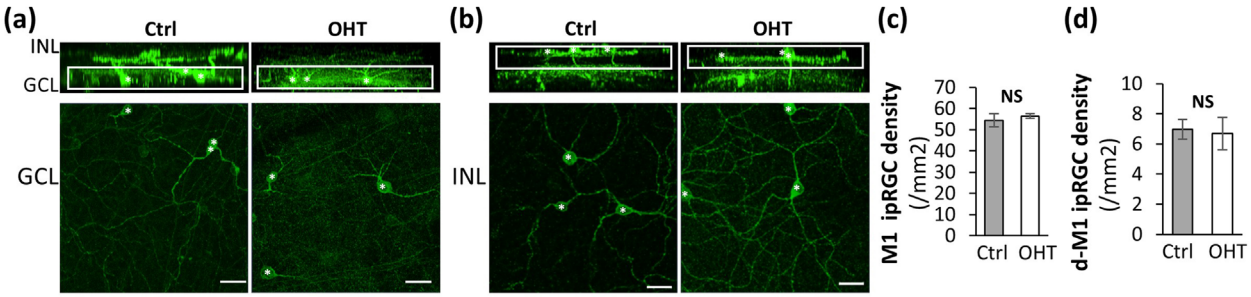

FIGURE 5 M1 ipRGC is resistant to the IOP elevation. (a) Identification of M1 ipRGCs by their dendritic patterning and location of somata. Z-stack confocal images of the flat-mounted retinas were projected to two-dimensional images and shown at the bottom. The extrapolated vertical view was shown on the top. White rectangles mark the ganglion cell layer (GCL). INL: inner nuclear layer. (b) Displaced melanopsin-positive cells in the INL. White rectangles mark the INL. Scale bar is 20 μm. (c, d) Quantifications of M1 density (c) and displaced M1 density (d). NS: not significant in the Mann–Whitney test. Data presented as mean ± *SEM*

equipped with running wheels and maintained in a 12h:12h L:D schedule. The mice were allowed to adapt for 10 days in the running wheel cages. We observed clear onsets of activity immediately after lights-off in both control and bilaterally lasered mice (Figure 6a). We then advanced the dark phase of the LD cycle by 6 h and monitored the wheel running behavior for 15 days. The entrainment was scored by a blind observer where re-entrainment was quantified as the number of days required to achieve a stable phase of entrainment to the advanced light cycle followed by two consecutive days of similar phase. Surprisingly, we found that the bilaterally lasered mice entrained significantly faster than control mice (controls: 8.8 ± 0.5 days, $n = 6$; OHT: 6.7 ± 0.7 days, $n = 6$, $p = .049$, Mann–Whitney test) (Figure 6a,b). To confirm this result, we performed another round of phase advance and found similar results (controls: 7.5 ± 0.4 days, $n = 6$; OHT: 5.8 ± 0.5 days, $n = 6$, $p = .04$, Mann–Whitney test). To test whether sensitivity of photoentrainment was altered, we performed a shift where the light intensity was reduced 60-fold from 100 to 1.5 μW/cm^2 (Figure 6c). We found no significant difference in the number of days required for re-entrainment between control and the bilaterally lasered mice (controls: 8.8 ± 0.5 days, $n = 6$; OHT: 7.8 ± 0.7 days, $n = 6$, $p = .22$, Mann–Whitney test) (Figure 6d).

We next tested whether the difference observed in re-entrainment rate is caused by a difference in circadian periods. The same animals were maintained under constant darkness for at least 2 weeks, and the stable free-running period was calculated across at least 10 days for each mouse (Figure 6e). We found no significant difference in circadian period between the control and bilaterally lasered mice (controls: 23.6 ± 0.02 h, $n = 6$; OHT: 23.6 ± 0.02 h, $n = 6$, $p = .81$, Mann–Whitney test) (Figure 6f).

After the circadian experiments (about 11 months post laser surgery), we examined the visual acuity (Figure 7a) and contrast sensitivity (Figure 7b) of the experimental and control animals. The

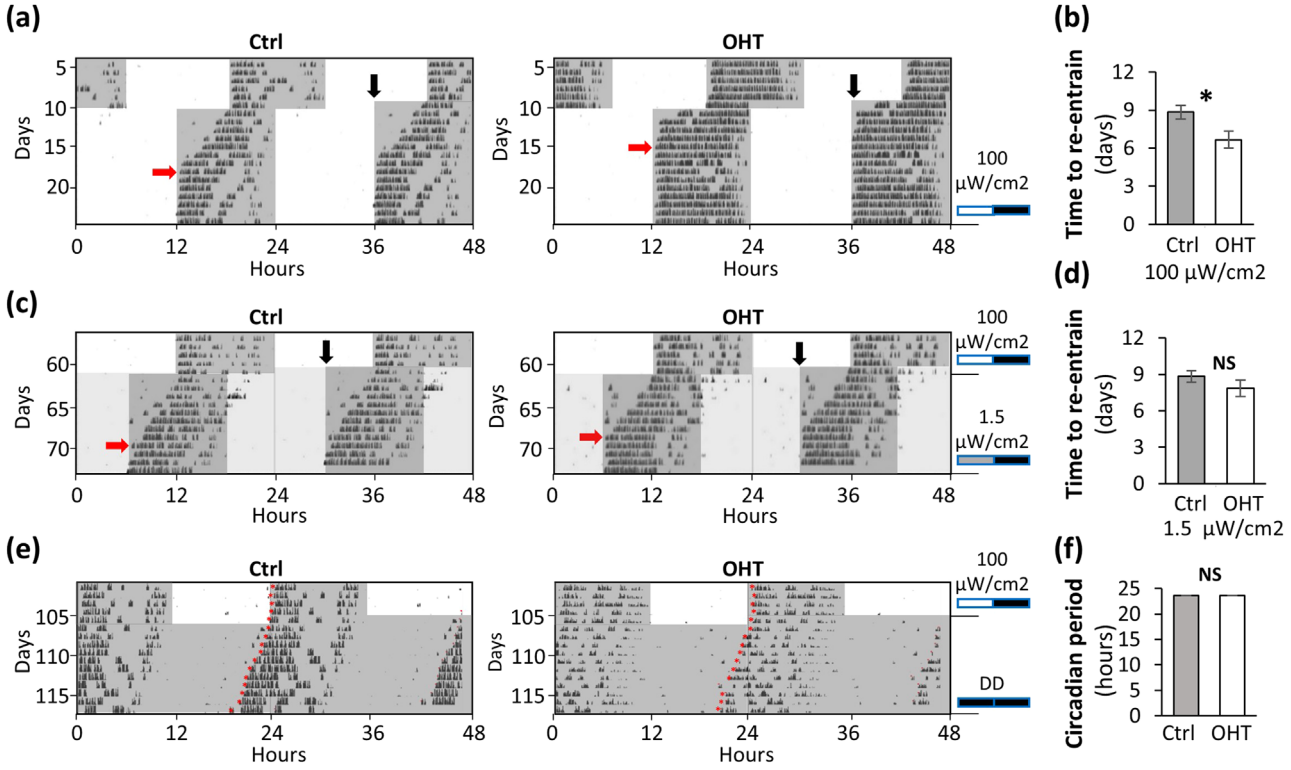

FIGURE 6 OHT mice exhibited a largely normal circadian re-entrainment behavior. (a) Examples of double plot actograms for a WT control and a bilaterally lasered mouse (OHT) under bright light intensity (a) or low light intensity (c) during light portion of the LD cycle. Six-hour phase-advance was performed to assess re-entrainment. White and light gray backgrounds indicate the light portions, and the dark gray backgrounds indicate the dark portions of the LD cycle, respectively. Red arrows point to the day when re-entrainment was observed. Black arrows point to the light shift. (b, d) Quantification of the average days it took for mice to re-entrain to the new LD cycle after phase-advance. (e) Examples of double plot actograms of circadian free run under constant darkness (DD) after day 105. Red asterisks mark the onset of activity on each day. (f) The average free running circadian periods for control and OHT mice. NS: not significant; $^{*}p < .05$ in the Mann–Whitney test. Data presented as mean ± *SEM*

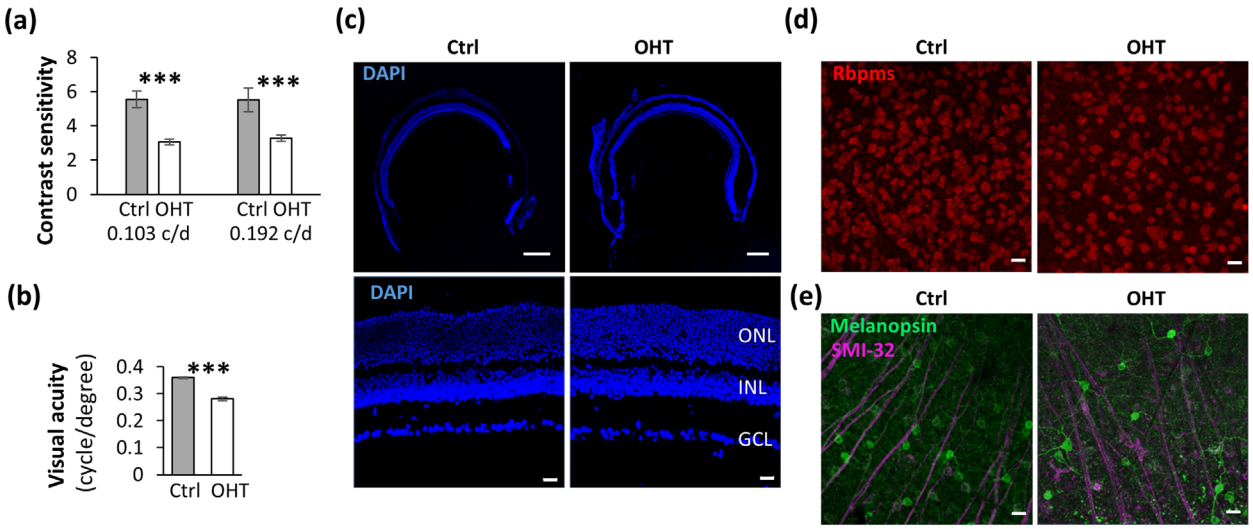

FIGURE 7 The overall retinal morphology was largely normal by 11 months post laser surgery, despite observed reduction in RGC density. (a, b) Contrast sensitivity (a) and visual acuity (b) of control and OHT mice 11-months post laser surgery. (c) Cross sections of control and bilaterally lasered OHT eye cups 11-months post laser surgery. Scale bar is 500 μm. Representative higher magnification images were shown below. Scale bar is 50 μm. (d, e) Flat-mounted retinas of control and OHT retina were stained with rbpms antibody (d) and antibodies against SMI-32 and melanopsin (e). Scale bar is 20 μm. $^{***}p < .001$ in the Mann–Whitney test. Data presented as mean ± *SEM*.

OHT mice exhibited a significantly reduced contrast sensitivity: at 0.103 c/d, the contrast sensitivity of OHT mice ($n = 12$ eyes) was 3.06 ± 0.18, and that of controls ($n = 12$ eyes) was 5.56 ± 0.49 ($p < .001$, Mann–Whitney test), At 0.192 c/d, the contrast sensitivity of OHT mice ($n = 12$ eyes) was 3.28 ± 0.18 and that of controls ($n = 12$ eyes) was 5.53 ± 0.69 ($p < .001$, Mann–Whitney test). Similarly, the visual acuity of OHT mice was significantly reduced compared to controls, which remained high (controls: 0.36 c/d, $n = 12$; OHT: 0.28 ± 0.01 c/d, $n = 12$; $p < .001$, Mann–Whitney test).

Finally, we analyzed the overall morphology of the retinas (Figure 7c). The laminar structure was largely normal in OHT eyes. As expected, we observed a decrease in RGC density as determined by rbpms labeling in the OHT retina (Figure 7d). We quantified two OHT retinas, and the overall density of the rbpms-positive cells in the OHT eyes was approximately 1674 cells/mm^2 at 12 months post laser photocoagulation, a 54.8% reduction compared to the control retina (3700 cells/mm^2, $n = 1$). Similarly, the density of melanopsin-positive ipRGCs was also reduced (Figure 7e) to 182.5 cells/mm^2 ($n = 2$), 13.5% lower than the control retina (211 cells/mm^2, $n = 1$).

4 | DISCUSSION

4.1 | Characterization of general RGC population and ipRGC subtypes

Rbpms is a general RGC marker that is expressed by most, if not all, RGCs in mouse retina (Rodriguez et al., 2014). We found that the anti-rbpms antibody labeled about half of all cells in the GCL as previously reported (Jeon et al., 1998). The other general RGC marker we used in this study, Brn3a, is present in 87% of all rbpms-positive RGCs (Figure 3a). We further assessed the general ipRGC population identified by the melanopsin antibody, which immunolabeled M1 through M4 (and possibly some M5) (Quattrochi et al., 2019; Stabio et al., 2018). We calculated a density of 219.6 cells/mm^2, which can be extrapolated to about 2800 cells per retina. This number agrees with a previous report of an estimated 2600 ipRGCs (Berson et al., 2010).

A total of six different ipRGC subtypes have been characterized, each with distinct morphology, physiology, and functions (Do, 2019; Duda et al., 2020). In the control retina, we calculated a density of 52.2 cells/mm^2 of M4 cells by anti-SMI32 and antimelanopsin antibodies. In one study by Schmidt and colleagues (Schmidt et al., 2014), an average of 571.6 total M4 cells were found in mouse retinas, which translates to about 45 cells/mm^2. Similar results were confirmed by another study where a total of 529 M4 cells were observed (Sonoda et al., 2020). We further classified displaced M1 cells by their specific dendritic lamination in the OFF sublamina of the IPL, similar to the M1 ipRGCs with perikarya in the GCL. We have calculated densities of 54.4 and 6.7 cells/mm^2 for M1 cells and displaced M1 cells, respectively. The total number of M1 cells is 54.4 + 6.7 = 61.1 cells/mm^2, which agrees with the previous finding by Berson and colleagues that the density of the total M1 cells was 63 cells/mm^2 (Berson et al., 2010). Together, our data show that these markers can assess accurately the general RGC population and ipRGC subtypes, thus enabling us to further examine their survivals in mice with chronic OHT.

4.2 | Subtype-dependent ipRGC degeneration in OHT mice

Glaucoma is characterized by progressive RGC cell degeneration and death (Feng, Zhao, et al., 2013; Chen et al., 2015; Quigley, 2016). We observed a 25.6% cell loss of Brn3a-positive RGCs and a 32.6% reduction in rbpms-positive RGC density 6–8 months post laser photocoagulation. Many studies have shown that ipRGCs are resistant to various disease insults (Duan et al., 2015; Feng, Zhao, et al., 2013; Chen et al., 2014; Tran et al., 2019). For example, in a chronic OHT model in rats, no substantial ipRGCs loss or change in dendritic arbor structure could be found after 3 months of sustained elevation of IOP, while a significant number of superior colliculus projecting RGCs degenerated (Li et al., 2006). In a mouse optic nerve crush model, ipRGCs also have been found to preferentially survive relative to other RGC types (Duan et al., 2015; Tran et al., 2019). Our results show that with chronic IOP elevation the general ipRGCs (all M1–M4, possibly some M5 and M6) density was reduced 16.5%, which is less than the 30% loss of the general RGC population.

The survival of ipRGCs may not be uniform among different subtypes. At 14 days, postoptic nerve crush injury, only a small number of M2 cells survived, but over 70% of M1 cells and over 80% of alpha RGCs labeled in a Kcng4-YFP transgenic line, including the M4 ipRGCs, survived (Duan et al., 2015). At 60-days postoptic nerve transection in rats, M1 cells comprised about 80% of all surviving RGCs (Pérez De Sevilla Müller et al., 2014). We also found no significant loss in M1 cells and displaced M1 cells in OHT mice; however, M4 cells suffered 25.7% loss. Other ipRGC subtypes, including M2s and possibly some M5 and M6s, also suffered about 23% cell loss (Table 2). This inconsistency may be explained by the different methods applied for RGC subtype categorization, as well as the differential survival of each subtype in different animal models. For example, Tran et al. (2019) quantified RGCs from single-cell samples dissociated from whole retinas, which provides a comprehensive profile of RGC survival but may also cause disproportionate representation of RGC types (Tran et al., 2019). Additionally, optic nerve crush injury or transection is an acute model of RGC damage, analyzed within a couple of weeks of crush, while chronic OHT induces slow and progressive RGC loss over months. Therefore, RGCs may respond differently to different types of disease insult (McKinnon et al., 2009). Interestingly, melanopsin overexpression in RGCs promoted axonal regeneration by activating the mammalian target of rapamycin (mTOR) pathway (Li et al., 2016). Taken together, we found that ipRGCs survived well with chronic OHT and this survival is subtype dependent. More work is needed to better understand the underlying molecular mechanisms of protection, degeneration, and regeneration which, in turn, will offer insights to develop neuroprotective treatments of glaucoma.

4.3 | Behavioral consequences of chronic OHT on circadian entrainments and visual acuity

As discussed, ipRGCs are involved in a broad range of image forming and nonimage forming functions (Do, 2019; Duda et al., 2020; Lucas et al., 2020). Thus, we further investigated how the subtype-specific loss of ipRGCs affects visual behaviors in mice suffering chronic OHT insult. It has been shown that M4 cells project to dLGN (Estevez et al., 2012) and contribute to contrast sensitivity aspects of image forming vision with and without rod/cone inputs (Ecker et al., 2010; Schmidt et al., 2014; Sonoda et al., 2020).

Specifically, following ablation of several ipRGC subtypes including the M4s, contrast sensitivity was significantly reduced at various spatial frequencies (Schmidt et al., 2014). The authors also observed that spatial frequencies at which significant deficits were found in these mice matched the spatial frequencies (0.05 and 0.09 c/d) to which M4s respond most strongly in isolated retina (Estevez et al., 2012), suggesting that M4s could contribute to contrast sensitivity. In the current study, we found a significant decrease in contrast sensitivity, which is also correlated with the significant loss of M4 cells in OHT eyes. Similarly, we also observed that our OHT mice exhibited greater reduction of contrast sensitivity at 0.103 c/d than 0.192 c/d (Figure 4c). Yet we cannot exclude that degeneration of other non-M4 RGCs may contribute to the change in contrast sensitivity in the OHT mice (Baden et al., 2016; Khani & Gollisch, 2017). M1 cells, on the other hand, project to the SCN, the master clock that regulates circadian photoentrainment, a nonimage forming function (Baver et al., 2008; Do, 2019; Vadnie & McClung, 2017). With little M1 loss under chronic OHT, we found no delay in circadian re-entrainment between nonocular hypertensive controls and OHT mice.

Note that when mice were subjected to a phase advance of a relatively bright LD cycle, the OHT mice established a stable phase of entrainment significantly faster than the age-matched controls. In a similar study using a rat OHT model, the authors found the opposite result where it took significantly more time for the OHT rat to re-entrain after phase advance (Drouyer et al., 2008). They also observed a significant reduction in RGC terminals in the SCN. These differences could be attributed to the intensity and duration of IOP elevation which may induce a different severity of RGC cell death. For example, IOP had been doubled for over 4 months in the rat glaucoma model, which led to a 50–70% reduction of RGC axon terminals in a majority of visual and nonvisual centers in the brain (Drouyer et al., 2008). By contrast, our mouse model exhibited a mild IOP elevation (about 20–30% increase) for a longer duration (from 3 months to up to a year).

The accelerated re-entrainment observed in mice with elevated IOP relative to normotensive controls was unexpected. We hypothesize that even a slight reduction of the direct photic input into the hypothalamus may cause an increase in the desynchrony among the cellular oscillators of the SCN. Such desynchrony speeds circadian entrainment in response to a shifted LD cycle. For example, the administration of vasoactive intestinal peptide (VIP) induces desynchrony or "phase tumbling" among SCN oscillator cells. If VIP is given prior to a shift in the LD cycle, the number of days required to re-entrain is halved compared to mice receiving vehicle injections (An et al., 2013). Although we did not observe a reduction in M1 cells in our bilaterally lasered mice, it remains possible that the synaptic input from M1 cells to the SCN was damaged under prolonged elevated IOP. In addition, the expression level of melanopsin as well as melanopsin activity could also affect re-entrainment rates. Melanopsin knockout mice exhibit reduced phase-shifting responses (Panda et al., 2002). The lack of C-terminal phosphorylation sites of the melanopsin molecule may also lead to faster re-entrainment (Somasundaram et al., 2017). Alternatively, we observed a decrease in M4 cells which project to the intergeniculate leaflet (IGL) (Ecker et al., 2010). The IGL, in turn, encodes irradiance and sends a projection to the SCN via the geniculohypothalamic tract (Morin, 2013; Yuan et al., 2018). Therefore, the degeneration of M4 cells could affect the IGL's modulation of the retinal input to the SCN and indirectly impact its behavioral output (Hanna et al., 2017).

The disruption of the circadian system observed in animal glaucoma models are also observed in patients. Primary open angle glaucoma (POAG) and primary angle-closure glaucoma patients often suffer mood and sleep disorders, and the severity is correlated with visual field impairment (Ciulla et al., 2020; Wang et al., 2013). Sleep efficiency assessed by polysomnographic recordings was significantly lowered (Gracitelli et al., 2015), and blood melatonin levels are higher in early morning in POAG patients (Ma et al., 2018). It will be of great interest to further understand the ipRGC-mediated neural circuits that account for the behavioral changes suffered by glaucoma patients. Such an understanding will lead to improved patient care and treatment as glaucoma develops and progresses.

ACKNOWLEDGMENTS

This study was funded by NIH grants R01EY029121 and R01EY026286. We thank Dr. Marta Grannonico for her technical support and fruitful discussions.

CONFLICTS OF INTEREST

The authors declare no conflicts of interest.

AUTHORS CONTRIBUTION

J.G., I.P., and X.L. designed the experiments; J.G., E.M. G., M.L., and J.M. carried out the experiments and data analysis; J.G., I.P., and X.L. wrote the manuscript, and J.G., E.M.G., M.L., J.M., I.P., and X.L. edited and approved the manuscript.

PEER REVIEW

The peer review history for this article is available at https://publons.com/publon/10.1002/cne.25293.

DATA AVAILABILITY STATEMENT

The data that support the findings of this study are available from the corresponding author upon reasonable request.

ORCID

Xiaorong Liu https://orcid.org/0000-0002-7655-6342

REFERENCES

An, S., Harang, R., Meeker, K., Granados-Fuentes, D., Tsai, C. A., Mazuski, C., Kim, J., Doyle, F. J., Petzold, L. R., & Herzog, E. D. (2013). A neuropeptide speeds circadian entrainment by reducing intercellular synchrony. *PNAS*, *110*(46), E4355–E4361. https://doi.org/10.1073/pnas.1307088110 http://doi.org/10.1073/pnas.1307088110

Baden, T., Berens, P., Franke, K., Román Rosón, M., Bethge, M., & Euler, T. (2016). The functional diversity of retinal ganglion cells in the mouse. *Nature*, *529*(7586), 345–350. https://doi.org/10.1038/nature16468

Baver, S. B., Pickard, G. E., Sollars, P. J., & Pickard, G. E. (2008). Two types of melanopsin retinal ganglion cell differentially innervate the hypothalamic suprachiasmatic nucleus and the olivary pretectal nucleus. *European Journal of Neuroscience*, *27*(7), 1763–1770. https://doi.org/10.1111/j.1460-9568.2008.06149.x

Berson, D. M., Castrucci, A. M., & Provencio, I. (2010). Morphology and mosaics of melanopsin-expressing retinal ganglion cell types in mice. *Journal of Comparative Neurology*, *518*(13), 2405–2422. https://doi.org/10.1002/cne.22381

Berson, D. M., Dunn, F. A., & Takao, M. (2002). Phototransduction by retinal ganglion cells that set the circadian clock. *Science*, *295*(5557), 1070–1073. https://doi.org/10.1126/science.1067262

Chen, S. - K., Badea, T. C., & Hattar, S. (2011). Photoentrainment and pupillary light reflex are mediated by distinct populations of ipRGCs. *Nature*, *476*(7358), 92–95. https://doi.org/10.1038/nature10206

Chen, H., Liu, X., & Tian, N. (2014). Subtype-dependent postnatal development of direction- and orientation-selective retinal ganglion cells in mice. *Journal of Neurophysiology*, *112*(9), 2092–2101. https://doi.org/10.1152/jn.00320.2014

Chen, H., Zhao, Y., Liu, M., Feng, L., Puyang, Z., Yi, J.i, Liang, P., Zhang, H. F., Cang, J., Troy, J. B., & Liu, X. (2015). Progressive degeneration of retinal and superior collicular functions in mice with sustained ocular hypertension. *Investigative Ophthalmology & Visual Science*, *56*(3), 1971–1984. https://doi.org/10.1167/iovs.14-15691

Ciulla, L., Moorthy, M., Mathew, S., Siesky, B., Verticchio Vercellin, A. C., Price, D., Januleviciene, I., & Harris, A. (2020). Circadian rhythm and glaucoma: What do we know. *Journal of Glaucoma*, *29*(2), 127–132 https://doi.org/10.1097/IJG.0000000000001402

Cui, Q., Ren, C., Sollars, P. J., Pickard, G. E., & So, K. - F. (2015). The injury resistant ability of melanopsin- expressing intrinsically photosensitive retinal ganglion cells. *Neuroscience*, *22*(284), 845–853. https://doi.org/10.1016/j.neuroscience.2014.11.002

Della Santina, L., Inman, D. M., Lupien, C. B., Horner, P. J., & Wong, R. O. L. (2013). Differential progression of structural and functional alterations in distinct retinal ganglion cell types in a mouse model of glaucoma. *Journal of Neuroscience*, *33*(44), 17444–17457. https://doi.org/10.1523/jneurosci.5461-12.2013

Do, M. T. H. (2019). Melanopsin and the Intrinsically photosensitive retinal ganglion cells: Biophysics to behavior. *Neuron*, *104*(2), 205–226. https://doi.org/10.1016/j.neuron.2019.07.016

Douglas, R. M., Alam, N. M., Silver, B. D., Mcgill, T. J., Tschetter, W. W., & Prusky, G. T. (2005). Independent visual threshold measurements in the two eyes of freely moving rats and mice using a virtual-reality optokinetic system. *Visual Neuroscience*, *22*(5), 677–684. https://doi.org/10.1017/S0952523805225166

Drouyer, E., Dkhissi-Benyahya, O., Chiquet, C., Woldemussie, E., Ruiz, G., Wheeler, L. A., Denis, P., & Cooper, H. M. (2008). Glaucoma alters the circadian timing system. *PloS One*, *3*(12), e3931. https://doi.org/10.1371/journal.pone.0003931

Duan, X., Qiao, M.u, Bei, F., Kim, I.n-J., He, Z., & Sanes, J. R. (2015). Subtype-specific regeneration of retinal ganglion cells following axotomy: Effects of osteopontin and mTOR signaling. *Neuron*, *85*(6), 1244–1256. https://doi.org/10.1016/j.neuron.2015.02.017

Duda, M., Domagalik, A., Orlowska-Feuer, P., Krzysztynska-Kuleta, O., Beldzik, E., Smyk, M. K., Stachurska, A., Oginska, H., Jeczmien-Lazur, J. S., Fafrowicz, M., Marek, T., Lewandowski, M. H., & Sarna, T. (2020). Melanopsin: From a small molecule to brain functions. *Neuroscience and Biobehavioral Reviews*, *113*, 190–203. https://doi.org/10.1016/j.neubiorev.2020.03.012

Ecker, J. L., Dumitrescu, O. N., Wong, K. Y., Alam, N. M., Chen, S.-K., Legates, T., Renna, J. M., Prusky, G. T., Berson, D. M., & Hattar, S. (2010). Melanopsin-expressing retinal ganglion-cell photoreceptors: Cellular diversity and role in pattern vision. *Neuron*, *67*(1), 49–60. https://doi.org/10.1016/J.NEURON.2010.05.023

Emanuel, A. J., Kapur, K., & Do, M. T. H. (2017). Biophysical variation within the M1 type of ganglion cell photoreceptor. *Cell Reports*, *21*(4), 1048–1062. https://doi.org/10.1016/j.celrep.2017.09.095

Estevez, M. E., Fogerson, P. M., Ilardi, M. C., Borghuis, B. G., Chan, E., Weng, S., Auferkorte, O. N., Demb, J. B., & Berson, D. M. (2012). Form and Function of the M4 Cell, an intrinsically photosensitive retinal ganglion cell type contributing to geniculocortical vision. *Journal of Neuroscience*, *32*(39), 13608–13620. https://doi.org/10.1523/JNEUROSCI.1422-12.2012

Feng, L., Chen, H., Suyeoka, G., & Liu, X. (2013). A laser-induced mouse model of chronic ocular hypertension to characterize visual defects. *Journal of Visualized Experiments*, (78), e50440. https://doi.org/10.3791/50440

Feng, L., Chen, H., Yi, J., Troy, J. B., Zhang, H. F., & Liu, X. (2016). Long-term protection of retinal ganglion cells and visual function by brain-derived neurotrophic factor in mice with ocular hypertension. *Investigative Ophthalmology & Visual Science*, *57*(8), 3793–3802. https://doi.org/10.1167/iovs.16-19825

Feng, L., Puyang, Z., Chen, H., Liang, P., Troy, J. B., & Liu, X. (2017). Overexpression of brain-derived neurotrophic factor protects large retinal ganglion cells after optic nerve crush in mice. *eNeuro*, *4*(1), ENEURO.0331–0316.2016. https://doi.org/10.1523/ENEURO.0331-16.2016

Feng, L., Zhao, Y., Yoshida, M., Chen, H., Yang, J. F., Kim, T. S., Cang, J., Troy, J. B., & Liu, X. (2013). Sustained ocular hypertension induces dendritic degeneration of mouse retinal ganglion cells that depends on cell type and location. *Investigative Ophthalmology & Visual Science*, *54*(2), 1106–1117. https://doi.org/10.1167/iovs.12-10791

Gracitelli, C. P. B., Duque-Chica, G. L., Roizenblatt, M., Moura, A. L. D.e A., Nagy, B. V., Ragot De Melo, G., Borba, P. D., Teixeira, S. H., Tufik, S., Ventura, D. F., & Paranhos, A. (2015). Intrinsically photosensitive retinal ganglion cell activity is associated with decreased sleep quality in patients with glaucoma. *Ophthalmology*, *122*(6), 1139–1148. https://doi.org/10.1016/j.ophtha.2015.02.030

Hanna, L., Walmsley, L., Pienaar, A., Howarth, M., & Brown, T. M. (2017). Geniculohypothalamic GABAergic projections gate suprachiasmatic nucleus responses to retinal input. *Journal of Physiology*, *595*(11), 3621–3649. https://doi.org/10.1113/JP273850

Hattar, S., Liao, H. - W., Takao, M., Berson, D. M., & Yau, K. - W. (2002). Melanopsin-containing retinal ganglion cells: Architecture, projections, and intrinsic photosensitivity. *Science*, *295*(5557), 1065–1070. https://doi.org/10.1126/science.1069609

Jain, V., Ravindran, E., & Dhingra, N. K. (2012). Differential expression of Brn3 transcription factors in intrinsically photosensitive retinal ganglion cells in mouse. *Journal of Comparative Neurology*, *520*(4), 742–755. https://doi.org/10.1002/cne.22765

Jeon, C.-J., Strettoi, E., & Masland, R. H. (1998). The major cell populations of the mouse retina. *Journal of Neuroscience*, *18*(21), 8936–8946. https://doi.org/10.1523/jneurosci.18-21-08936.1998

Khani, M. H., & Gollisch, T. (2017). Diversity in spatial scope of contrast adaptation among mouse retinal ganglion cells. *Journal of Neurophysiology*, *118*(6), 3024–3043. https://doi.org/10.1152/jn.00529.2017

Li, R. S., Chen, B.-Y.u, Tay, D. K., Chan, H. H. L., Pu, M.-L., & So, K.-F. (2006). Melanopsin-expressing retinal ganglion cells are more injury-resistant in a chronic ocular hypertension model. *Investigative Ophthalmology & Visual Science*, *47*(7), 2951–2958. https://doi.org/10.1167/iovs.05-1295

Li, S., Yang, C., Zhang, L.i, Gao, X., Wang, X., Liu, W., Wang, Y., Jiang, S., Wong, Y. H., Zhang, Y., & Liu, K. (2016). Promoting axon regeneration in the adult CNS by modulation of the melanopsin/GPCR signaling. *PNAS*, *113*(7), 1937–1942. https://doi.org/10.1073/pnas.1523645113

Lucas, R. J., Allen, A. E., Milosavljevic, N., Storchi, R., & Woelders, T. (2020). Can We See with Melanopsin? *Annual Review of Vision SCIENCE*, *6*, 453–468, https://doi.org/10.1146/annurev-vision-030320-041239

Ma, X. P., Shen, M. Y., Shen, G. L., Qi, Q. R., & Sun, X. H. (2018). Melatonin concentrations in serum of primary glaucoma patients. *International Journal of Ophthalmology*, *11*(8), 1337–1341. https://doi.org/10.18240/ijo.2018.08.14

McKinnon, S. J., Schlamp, C. L., & Nickells, R. W. (2009). Mouse models of retinal ganglion cell death and glaucoma. *Experimental Eye Research*, *88*(4), 816–824. https://doi.org/10.1016/j.exer.2008.12.002

Morin, L. P. (2013). Neuroanatomy of the extended circadian rhythm system. *Experimental Neurology*, *243*, 4–20. https://doi.org/10.1016/j.expneurol.2012.06.026

Pan, L., Yang, Z., Feng, L., & Gan, L. (2005). Functional equivalence of Brn3 POU-domain transcription factors in mouse retinal neurogenesis. *Development (Cambridge, England)*, *132*(4), 703–712. https://doi.org/10.1242/dev.01646

Panda, S., Sato, T. K., Castrucci, A. M., Rollag, M. D., Degrip, W. J., Hogenesch, J. B., Provencio, I., & Kay, S. A. (2002). Melanopsin (Opn4) requirement for normal light-induced circadian phase shifting. *Science*, *298*(5601), 2213–2216. https://doi.org/10.1126/science.1076848

Pérez De Sevilla Müller, L., Sargoy, A., Rodriguez, A. R., & Brecha, N. C. (2014). Melanopsin ganglion cells are the most resistant retinal ganglion cell type to axonal injury in the rat retina. *PloS One*, *9*(3), e93274. https://doi.org/10.1371/journal.pone.0093274

Prusky, G. T., Alam, N. M., Beekman, S., & Douglas, R. M. (2004). Rapid quantification of adult and developing mouse spatial vision using a virtual optomotor system. *Investigative Ophthalmology & Visual Science*, *45*(12), 4611–4616. https://doi.org/10.1167/iovs.04-0541

Quattrochi, L. E., Stabio, M. E., Kim, I., Ilardi, M. C., Michelle Fogerson, P., Leyrer, M. L., & Berson, D. M. (2019). The M6 cell: A small-field bistratified photosensitive retinal ganglion cell. *Journal of Comparative Neurology*, *527*(1), 297–311. https://doi.org/10.1002/cne.24556

Quigley, H. A. (2016). Understanding glaucomatous optic neuropathy: The synergy between clinical observation and investigation. *Annual Review of Vision Science*, *2*(1), 235–254. https://doi.org/10.1146/annurev-vision-111815-114417

Rangarajan, K. V., Lawhn-Heath, C., Feng, L., Kim, T. S., Cang, J., & Liu, X. (2011). Detection of visual deficits in aging DBA/2J mice by two behavioral assays. *Current Eye Research*, *36*(5), 481–491. https://doi.org/10.3109/02713683.2010.549600

Rodriguez, A. R., De Sevilla Müller, L. P., & Brecha, N. C. (2014). The RNA binding protein RBPMS is a selective marker of ganglion cells in the mammalian retina. *Journal of Comparative Neurology*, *522*(6), 1411–1443 https://doi.org/10.1002/cne.23521

Sanes, J. R., & Masland, R. H. (2015). the types of retinal ganglion cells: Current status and implications for neuronal classification. *Annual Review of Neuroscience*, *38*(1), 221–246. https://doi.org/10.1146/annurev-neuro-071714-034120

Schmidt, T. M., Alam, N. M., Chen, S., Kofuji, P., Li, W., Prusky, G. T., & Hattar, S. (2014). A role for melanopsin in alpha retinal ganglion cells and contrast detection. *Neuron*, *82*(4), 781–788. https://doi.org/10.1016/j.neuron.2014.03.022

Somasundaram, P., Wyrick, G. R., Fernandez, D. C., Ghahari, A., Pinhal, C. M., Simmonds Richardson, M., Rupp, A. C., Cui, L., Wu, Z., Brown, R. L., Badea, T. C., Hattar, S., & Robinson, P. R. (2017). C-terminal phosphorylation regulates the kinetics of a subset of melanopsin-mediated behaviors in mice. *PNAS*, *114*(10), 2741–2746. https://doi.org/10.1073/pnas.1611893114

Tsui, D. K.a-K., Yau, K.-K., & Tang, C.-N. (2020). Crosstalk: The diversity of melanopsin ganglion cell types has begun to challenge the canonical divide between image-forming and non-image-forming vision. *Journal of Comparative Neurology*, *528*, 127–128. https://doi.org/10.1111/1744-1633.12020

Sonoda, T., Okabe, Y., & Schmidt, T. M. (2020). Overlapping morphological and functional properties between M4 and M5 intrinsically photosensitive retinal ganglion cells. *Journal of Comparative Neurology*, *528*(6), 1028–1040. https://doi.org/10.1002/cne.24806

Stabio, M. E., Sabbah, S., Quattrochi, L. E., Ilardi, M. C., Fogerson, P. M., Leyrer, M. L., Kim, M. T., Kim, I., Schiel, M., Renna, J. M., Briggman, K. L., & Berson, D. M. (2018). The M5 cell: A color-opponent intrinsically photosensitive retinal ganglion cell. *Neuron*, *97*(1), 150–163.e4. https://doi.org/10.1016/j.neuron.2017.11.030

Tham, Y.-C., Li, X., Wong, T. Y., Quigley, H. A., Aung, T., & Cheng, C.-Y.u (2014). Global prevalence of glaucoma and projections of glaucoma burden through 2040. *Ophthalmology*, *121*(11), 2081–2090. https://doi.org/10.1016/j.ophtha.2014.05.013

Thomson, B. R., Grannonico, M., Liu, F., Liu, M., Mendapara, P., Xu, Y., Liu, X., & Quaggin, S. E. (2020). Angiopoietin-1 knockout mice as a genetic model of open-angle glaucoma. *Translational Vision Science & Technology*, *9*(4), 16. https://doi.org/10.1167/tvst.9.4.16

Tran, N. M., Shekhar, K., Whitney, I. E., Jacobi, A., Benhar, I., Hong, G., Yan, W., Adiconis, X., Arnold, M. E., Lee, J. M., Levin, J. Z., Lin, D., Wang, C., Lieber, C. M., Regev, A., He, Z., & Sanes, J. R. (2019). Single-cell profiles of retinal ganglion cells differing in resilience to injury reveal neuroprotective genes. *Neuron*, *104*(6), 1039–1055.e12. https://doi.org/10.1016/j.neuron.2019.11.006

Vadnie, C. A., & Mcclung, C. A. (2017). Circadian rhythm disturbances in mood disorders: Insights into the role of the suprachiasmatic nucleus. *Neural Plasticity*, *2017*, 1–28. https://doi.org/10.1155/2017/1504507

Voinescu, P. E., Kay, J. N., & Sanes, J. R. (2009). Birthdays of retinal amacrine cell subtypes are systematically related to their molecular identity and soma position. *Journal of Comparative Neurology*, *517*(5), 737–750. https://doi.org/10.1002/cne.22200

Wang, H., Zhang, Y.e, Ding, J., & Wang, N. (2013). Changes in the Circadian Rhythm in Patients with Primary Glaucoma. *PloS One*, *8*(4), e62841. https://doi.org/10.1371/journal.pone.0062841

Xiang, M., Zhou, L., Macke, J., Yoshioka, T., Hendry, S., Eddy, R., Shows, T., & Nathans, J. (1995). The Brn-3 family of POU-domain factors: Primary structure, binding specificity, and expression in subsets of retinal ganglion cells and somatosensory neurons. *Journal of Neuroscience*, *15*(7), 4762–4785. https://doi.org/10.1523/jneurosci.15-07-04762.1995

Yuan, X.-S., Wei, H.-H., Xu, W., Wang, L.u, Qu, W.-M., Li, R.-X., & Huang, Z.-L. (2018). Whole-brain monosynaptic afferent projections to the cholecystokinin neurons of the suprachiasmatic nucleus. *Frontiers in Neuroscience.*, *12*, 807. https://doi.org/10.3389/fnins.2018.00807

How to cite this article: Gao, J., Griner, E. M., Liu, M., Moy, J., Provencio, I, & Liu, X. (2022). Differential effects of experimental glaucoma on intrinsically photosensitive retinal ganglion cells in mice. *J Comp Neurol*, 1–13. https://doi.org/10.1002/cne.25293